Distribution of Hydrophobic Probe Molecules in Lipid Bilayers. 1. Monte Carlo Dynamics Computer Simulations

M. A. M. J. van Zandvoort, H. C. Gerritsen, and Y. K. Levine*

Department of Molecular Biophysics, Debye Institute, Buys Ballot Laboratory, Utrecht University, P.O. Box 80.000, 3508 TA, Utrecht, The Netherlands

Received: October 31, 1996; In Final Form: February 19, 1997[⊗]

Lattice dynamics techniques are used to simulate the orientational dynamics of the hydrophobic probe molecules 1,6-diphenyl-1,3,5-hexatriene DPH and perylene in lipid bilayer systems. It is shown that these molecules are essentially found in two distinct environments: in the middle of the bilayer and in the two regions near the bilayer interfaces. This partition arises from the competition between the entropic effects of free volume and the interaction of the probes with the lipid molecules. Each probe population exhibits a distinct orientational and dynamical behavior. The probe molecules move through the bilayer on a time scale slow compared to their rotational motions such that the two populations are effectively in dynamic equilibrium. The simulations reveal, furthermore, inherent ambiguities in the analysis of time-resolved fluorescence anisotropy measurements on such heterogeneous systems. This problem is illustrated in the accompanying paper, where a detailed analysis of time-resolved fluorescence anisotropy of perylene molecules in lipid vesicle systems is presented.

Introduction

The study of the orientational order and rotational dynamics of the lipid hydrocarbon chains in membrane systems is derived from the wish to understand which physical processes underlie biological functions.[1−3] Although NMR spectroscopy yields the most direct information, it suffers from the distinct disadvantage that the investigations rely on the availability of selectively deuterated molecules. An experimentally convenient alternative is provided by techniques such as fluorescence depolarization and electron spin resonance (ESR), which employ extraneous probe molecules incorporated in the membrane structure. These techniques are particularly suitable for studying the molecular order and dynamics in lipid membranes, since their intrinsic time window covers the range of rotational motions of the probe molecules.

The starting point in the interpretation of the experimental observations is a model for the stochastic rotational motions of the probe.[4−6] To this end, it is common to assume that each probe molecule experiences a local orienting potential imposed on it by the surrounding lipid molecules. The orientational distribution function of the molecules is given simply by the Boltzmann distribution corresponding to this orienting potential.[6,7] The most successful motional models for describing the fluorescence depolarization decays and the ESR line shapes are the Brownian rotational siffusion model (BRD)[5−7] and particularly its extension, the compound motion model (CM).[6,8,9] The former describes small-step rotational diffusion of a probe molecule under the influence of an effective orienting potential. The CM model postulates that the probe molecules are confined to the free-volume cavities in the bilayer structure. Within the boundaries of these cavities the probes exhibit fast rotational motions. However, larger angular excursions are only possible upon a rotation of the cavities as a whole.

In applying these concepts to the quantitative analysis of experimental data, one has to bear in mind that some probes, such as the fluorescent molecule TMA-DPH[22] and cholestane spin label (CSL) are anchored to the aqueous interface of the membrane structure. Others such as the cylindrical fluorescent molecules DPH or the planar perylenes are free to access every region of the bilayer interior. It has been recently shown that the experimental data for DPH can be equally well described by the BRD and CM models as well as by assuming the molecules to exist as two populations with distinct order and dynamics in the bilayer, each characterized by its own fluorescence lifetime.[10] One population corresponds to probes intercalated between the lipid chains and the other to probes in the center of the bilayer. The basic premise of this latter model is that the orienting potential acting on the probes depends on their position relative to the bilayer surface. Unfortunately, the experimental data cannot discriminate between these descriptions. Nevertheless, the two-populations model is appealing in that it rests on the link between the complex fluorescence intensity decay and the localization of the probe populations present in the bilayer.

The question thus remains as to what information is furnished by probe molecules such as DPH and perylene about the membrane system. The resolution of this problem calls for an approach in which the behavior of both the lipid molecules and the fluorescent molecules is monitored. In contrast to any experimental method, this can be achieved in a straightforward way with computer simulation techniques. We have recently shown that Monte Carlo dynamics (MCD)[6,11−13] methods can be used to simulate the principal structural features of lipid bilayers as well as the behavior of elongated rigid probe molecules anchored to the interface of the lipid bilayer above the phase transition of the hydrocarbon chains. The simulations thus mimic the behavior of the fluorescent probe TMA-DPH[12] and cholestane spin label (CSL).[13]

The MCD method rests on the assumption that the conformational dynamics of the lipid chains can be described as the superposition of local structural arrangements involving small chain segments. This is realized in a computationally efficient way by making use of a lattice. The MCD calculations were implemented taking into account only the conformational energy of the chains and excluded volume effects. The simulations reproduced the electron density profile of the bilayers obtained from X-ray diffraction experiments, the ^{2}H NMR order param-

* Corresponding author.
[⊗] Abstract published in *Advance ACS Abstracts,* April 1, 1997.

S1089-5647(96)03414-1 CCC: $14.00

eter profile of the C−D bonds along lipid chains, as well as their mobility gradient. In addition, the simulations accounted for the effects of cholesterol molecules on the conformational order and dynamics of the lipids. An important prediction of the simulations is that the free volume in the bilayer increases significantly on moving from its interface toward the center.[11,12] The high free volume in the middle of the bilayer is the result of the imperfect packing of the flexible hydrocarbon chains of the two opposing monolayers.

The MCD simulations of rigid probe molecules anchored to the bilayer interface underpin the CM model and show that the orientational order of the probe is primarily determined by the behavior of long chain segments. Probes not anchored at the interface of the bilayer will tend to accumulate in the center of the bilayer, with their long axes oriented preferentially parallel to the surface.[12] This tendency, however, is expected to be counteracted by the interaction of the guest molecules with the surrounding lipid chains. Here, we shall model such interactions by subjecting the probe molecules to an ad hoc effective burial potential in the lipid bilayer. This approach has been previously used in computer simulations of protein structure to account for the location of hydrophilic and hydrophobic groups relative to the center of mass of globular proteins,[14] as well as in studies of the insertion of peptide chains into lipid bilayers.[15]

It will be shown that under the effect of a burial potential, DPH and perylene molecules are essentially found in two distinct environments: in the middle of the bilayer and in the two regions near the bilayer interfaces. This arises from the competition between the entropic effects of free volume and the counteracting energetics. Each probe population exhibits a distinct orientational and dynamical behavior. The probe molecules move through the bilayer on a time scale slow compared to their rotational motions such that the two populations are effectively in dynamic equilibrium. The simulations reveal, furthermore, inherent ambiguities in the analysis of time-resolved fluorescence anisotropy measurements on such heterogeneous system. This problem is illustrated in the accompanying paper,[16] where the analysis of time-resolved fluorescence anisotropy of perylene molecules in lipid vesicle systems is presented.

Method of Simulation

The MCD technique for simulating the dynamic behavior of hydrocarbon chains of lipids in monolayer and bilayer structures has been discussed and validated in detail previously.[11−13] Only the salient points will be summarized here. Importantly, the simulations described below use a more realistic implementation of excluded volume effects.

Lattice Representation of Lipid Chains. The method makes use of a representation of hydrocarbon chains on a cubic lattice. The bilayer was constructed of two monolayers each containing 255 model lipid chains consisting of 16 atoms. The bilayer was contained in a Monte Carlo box having a square cross-section in the *XY*-plane of the lattice and extending along the positive *Z*-axis. The interfaces of the monolayers forming the bilayer system were taken to lie parallel to the *XY*-plane of the lattice and centered at heights $Z = -{}^1/_2T_{bil}$ and $Z = {}^1/_2T_{bil}$, with T_{bil} the bilayer thickness. The headgroups were attached to the interfaces with a harmonic potential ($k = 0.5kT$) to mimic the diffuse nature of the bilayer structure: $U(z) = k(|z| - {}^1/_2T_{bil})^2$. Moreover, each methylene group was subjected to the same repulsive harmonic potential on crossing the interface, i.e., when $|z| > {}^1/_2T_{bil}$. Periodic boundary conditions were imposed on the positions of all the atoms in the *XY*-plane only.

The excluded volume effects were implemented by assigning an impenetrable spherical envelope of radius 2.1 lattice units to each of the methylene atoms. Each lattice unit corresponds to a distance of 0.069 nm. The headgroups were represented by spheres with a radius of 2.7 lattice units. This larger excluded volume envelope of the headgroups accounts for their interaction with surrounding water molecules. Intrachain effects were simulated by rejecting any chain conformations exhibiting overlap of spheres representing atoms separated by more than three bonds in the chain. The interchain excluded volume effects were implemented by occupying all the lattice positions within the sphere representing the atom.

Local Conformational Moves. The conformational dynamics of the lipid chain is considered to arise from a superposition of local structural rearrangements constrained by the bond lengths. For example, in a polymethylene chain the elementary move involves the transfer of a pair of adjacent atoms, $-C_1-C_2-$, chosen at random to different lattice sites. However, the motions of the headgroup atoms were penalized by a factor of 0.02 to mimic the effects of their interaction with the aqueous phase. This slowed the lateral translational motion of the chains across the *XY*-plane to a time scale longer than that of the conformational moves.

Each random elementary move attempted by the atoms is subjected to two acceptance tests: (1) a move is only accepted if the final lattice positions of the excluded volume envelopes of the atoms are unoccupied; (2) the new configuration was accepted with a probability *P* given by the symmetric scheme

$$P = \frac{\exp(-E_{new}/(kT))}{\{\exp(-E_{old}/(kT)) + \exp(-E_{new}/(kT))\}}$$

We note that the effects of temperature enter the simulation only through this acceptance test.

Probe Molecule Representation. The DPH molecules were represented as rigid, solid objects 19 lattice units long with a square cross section with a side of 7 lattice units. Two DPH molecules were used in the simulations, one intercalated between the molecules of each monolayer at the start of the run. Note that this results in a probe concentration comparable to the experimental ratio ∼1:250. Only a single perylene molecule was embedded in the bilayer. The molecule was taken to be a solid square object of side 17 lattice units and a thickness of 4 lattice units. Both types of probe molecules were allowed to undergo small step random rotations about their center of mass as well as rigid body translational motions using standard algorithms.[17] They were confined within the bilayer structure by subjecting them to a repulsive harmonic potential ($k = 0.5kT$) if any part of the molecule protruded beyond the bilayer interface.

MCD Algorithm. The Monte Carlo dynamics algorithm for a bilayer containing *M* hydrocarbon chains each consisting of *N* atoms was executed in the following way. Given a particular configuration of the bilayer, Ω_j, $M \times N$ local conformational moves are attempted at random with each atom in the system having an equal chance of being picked. This was followed by an attempted move of the probe molecules. These moves generate a new configuration of the bilayer, Ω_{j+1}. The cycle is now repeated using Ω_{j+1} as the starting configuration. The fundamental time-step of the algorithm is defined as the time required for the bilayer to undergo a transition from configuration Ω_j to Ω_{j+1}. It is important to realize that this time step of the MCD algorithm cannot be related to an absolute scale.

We have typically generated a trajectory consisting of 8×10^4 bilayer configurations each separated by five elementary time-steps at a temperature of 400 K. The number of elementary time-steps separating the configurations stored was chosen to

ensure the complete decay of the time correlation functions (see below) to equilibrium within a time window of 2000 steps along the trajectory.

The calculation for a bilayer of 510 chains each consisting of 16 atoms and containing either 2 DPH probes or a single perylene molecule required around 24 h CPU time on a Silicon Graphics Indy workstation. With this choice, the statistical fluctuations in the calculated order parameters $\langle P_2 \rangle$ and $\langle P_4 \rangle$ for the probe molecules and chains obtained from runs starting with different initial bilayer configurations varied by less than 3%. Furthermore, the decay of the time correlation functions for every atom of the chain and for the axes of the probe molecules was found to be independent of the sampling frequency of the trajectory generated.

Time Correlation Functions. To characterize the rotational motions of the probe molecules, we have used the trajectories to evaluate the orientational time correlation functions $G_{00}^{L}(t)$

$$G_{00}^{L}(t) = \langle\langle P_{\mathrm{L}}\{\bar{m}(0)\cdot\bar{m}(t)\}\rangle\rangle; \quad L = 1, 2 \tag{1}$$

Here, P_{L} denotes the Legendre polynomial of rank L and $\bar{m}(t')$ is the vector corresponding to the *x*-, *y*-, or *z*-axis of the probe molecule at time t' in the bilayer frame. The double bracket indicates an average over the probe or lipid molecules. The time t is measured in steps along the trajectory of bilayer configurations rather than in elementary time steps of the MCD algorithm. The time-correlation function $G_{00}^{2}(t)$ is monitored in fluorescence depolarization experiments on macroscopically isotropic lipid vesicle systems.[5,6,8] Although the first rank correlation function $G_{00}^{1}(t)$ is not accessible experimentally, its decay reflects the tumbling motion of the molecular axes, in particular "head-over-heels" modes of motion.

These time-correlation functions were fitted to the predictions of the CM model using a nonlinear Marquardt optimization procedure using the symmetric orienting potential

$$U(\beta) = -kT[\lambda_2 P_2(\beta) + \lambda_4 P_4(\beta)] \tag{2}$$

for describing the orientational behavior of the cone containing the cylindrical probe molecule. We note that the order parameters $\langle P_2 \rangle$ and $\langle P_4 \rangle$ are uniquely determined by the pair of parameters λ_2 and λ_4.

Results and Discussion

The simulations were carried out on a model bilayer confined to an MC box of side 144 lattice units, corresponding to about 0.38 nm^2/chain, at a temperature of 400 K. The bilayer thickness was kept constant at 50 lattice units, about 3.5 nm. Under these conditions the $\langle P_2 \rangle$ order parameter profile of the C−D bonds down the length of the chain was in excellent agreement with the experimental one found for bilayers of potassium palmitate (K−C_{16}) at 395 K.[18] The order parameters of the C−D bonds increase on reducing the size of the MC box or the temperature. Similarly, increasing the effective area/molecule or the temperature induces disorder in the bilayer chains.

DPH Probes. *A. Orientational Distribution Functions*. The two probe molecules included in the simulations were subjected to an ad hoc repulsive harmonic burial potential relative to the center of the bilayer at $z = 0$: $U_{\mathrm{B}} = -\kappa z_{\mathrm{CM}}^2$ with z_{cm} the position of the molecular center of mass. The distribution of the centers of mass of the probes through the bilayer is shown in Figure 1. It appears that the centers of the probes are found preferentially either in a region of width 22 lattice units around the center of the bilayer or in two regions each of width 14 lattice units near the interfaces at $Z = \pm 25$ lattice units. The proportion of probe molecules in the central region decreases significantly on increasing the strength of the burial potential from $0 \le \kappa \le 0.04kT$: 95% and 5%, respectively. Equal probe populations in the center and in the interfacial regions of the bilayer are found for a potential of strength $\kappa = 0.03kT$.

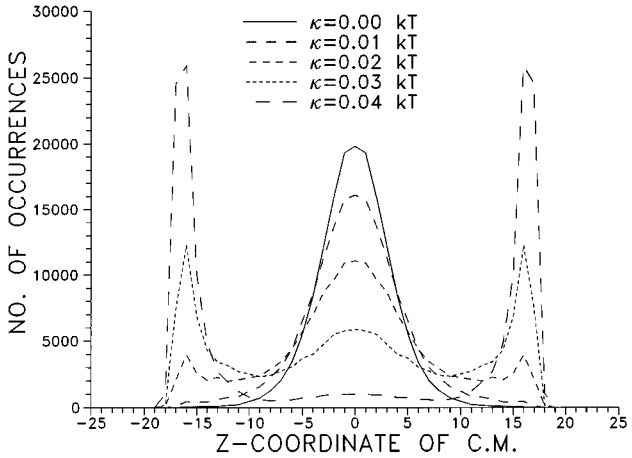

Figure 1. Distribution of the positions of the centers of mass of the model DPH molecules in the bilayer for different strengths of the burial potneial.

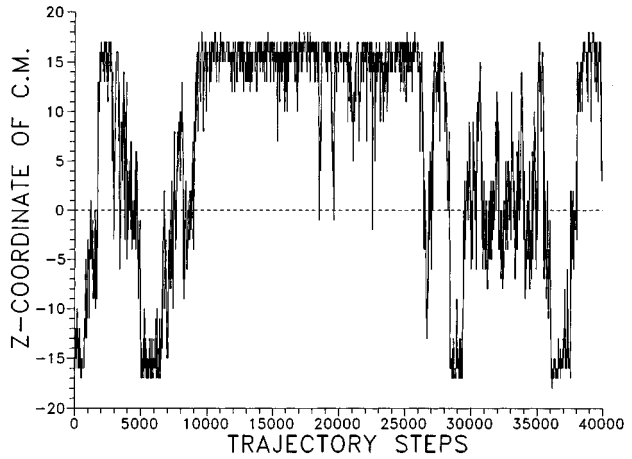

Figure 2. Typical variation of the position of the center of mass of a model DPH molecule in the bilayer during a simulation run.

The position of the center of a given probe molecule in the bilayer changes during the course of the simulation run so that a dynamic equilibrium exists between the two populations (Figure 2). The motion of the center of the molecule is found to be slower than the reorientational motions (see below). We note that the strength of the repulsive burial potential is an order of magnitude smaller than that of the harmonic potentials used to anchor the headgroups to the bilayer interface and to confine the chains to the bilayer interior.

The simulation runs provide the orientational distribution function of the probes localized at different depths with respect to the bilayer interface. We have here chosen to keep track of the orientational distributions of molecules in the central and interfacial regions of the bilayer corresponding to those found above for the localization of their centers. The orientational distribution functions of probes localized in the center of the bilayer was found to be broad with a maximum near $\beta = \pi/2$ (Figure 3). Here, β denotes the angle between the long axes of the probes and the normal to the bilayer surface. The orientational distribution functions, $f(\beta)$, shown in this paper were obtained by fitting the number density obtained in the simulation to a Boltzmann distribution using the orienting potential of eq

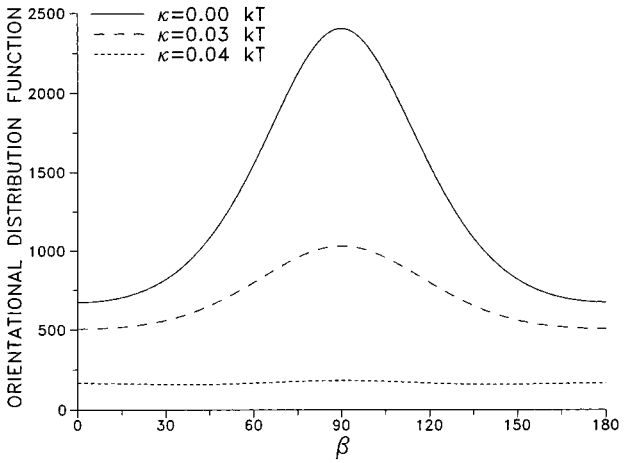

Figure 3. Orientational distribution function of the DPH population localized in the middle of the bilayer for different strengths of the burial potential.

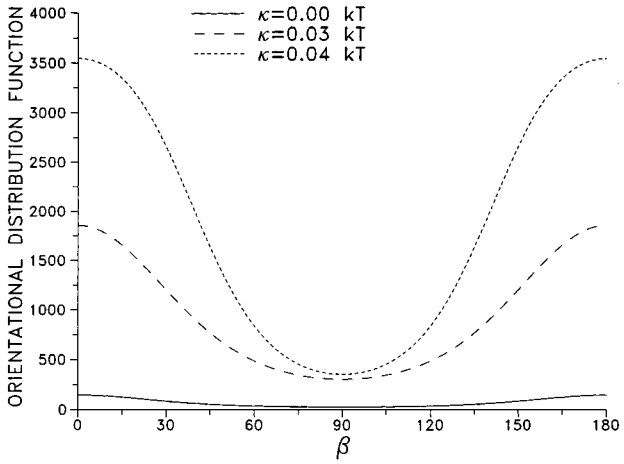

Figure 4. Orientational distribution function of the DPH population localized in the interfacial regions of the bilayer for different strengths of the burial potential.

2. The distribution functions are characterized by negative values of the order parameter $\langle P_2 \rangle$; $\langle P_2 \rangle = -0.16$ in the absence of a burial potential. In marked contrast, probes localized in the top half of each monolayer exhibited a narrower distribution function, peaking at $\beta = 0$ (Figure 4). For a burial potential of strength $\kappa = 0.04kT$, $\langle P_2 \rangle = 0.34$.

These results show that the probes localized in the middle of the bilayer are preferentially oriented with their long axes parallel to the bilayer surface. On the other hand, the probes in the interfacial regions interdigitate between the chains of the bilayer, and their axes consequently undertake orientations preferentially along the normal to the bilayer surface. This implies that the effective orienting potential acting on the probe depends on its position relative to the bilayer interface. Indeed, a finer binning of the positions of the probe centers shows that the orientational distribution function of the probes changes continuously on moving from the interface toward the middle of the bilayer.

We note that a reduction in the size of the MC box, whether or not accompanied by a lowering of the temperature, results in sharper orientational distribution functions of both populations around their respective maxima. We thus find $\langle P_2 \rangle$ for the central probe population to become even more negative, while $\langle P_2 \rangle$ for probes in the interfacial regions takes on larger values. It is important to realize that a perfect alignment of the long molecular axes parallel to the bilayer interface is characterized by $\langle P_2 \rangle = -0.5$.

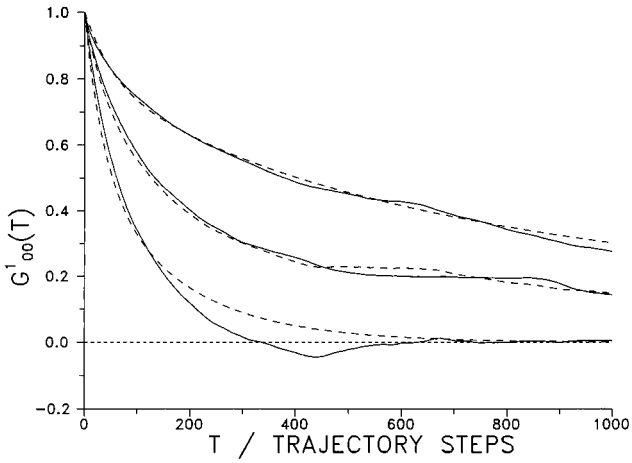

Figure 5. Decay of the first-rank time correlation function $G^1_{00}(t)$ of DPH molecules in the lipid bilayer (continuous lines): population in the middle of the bilayer ($\kappa = 0$) (bottom); population in the interfacial regions ($\kappa = 0.04kT$) (top); a mixed population ($\kappa = 0.03kT$) (center). The fits to the CM model (dashed lines) are shown for the populations in the middle (top) and interfacial regions (bottom) as is the weighted sum of the correlation functions (center).

Finally, we stress that the length of the probe used in the simulation determines the details of the findings reported above. The probe molecules can only change position in the bilayer structure provided there is a region of free volume of an appropriate geometrical shape to accommodate them. The shape, size, and orientation of these free volume regions fluctuate with time, since they are bounded by the flexible hydrocarbon chains. The bilayer structure contains a higher proportion of small free volume regions of a regular shape than large regions. Consequently, short cylindrical probe molecules will experience less hindrance to motion, exhibit a more limited orientational order, and be more susceptible to the effects of the burial potential than long probe molecules. This is also reflected in the detailed behavior of the bulkier perylene molecules as will be shown below.

B. Reorientational Motions. We shall here consider the decay of the first- and second-rank time correlation functions, $G^1_{00}(t)$ and $G^2_{00}(t)$, calculated from the trajectories of the stochastic probe orientations. These calculations take no account of the depth of the probe within the bilayer and consequently correspond to the experimental situation. Only the correlation functions of the long molecular axis of the model DPH molecule will be considered for different strengths of the burial potential. We note that the second-rank time correlation function, $G^2_{00}(t)$, of this axis is monitored in a fluorescence anisotropy experiment.[5] The first-rank correlation function $G^1_{00}(t)$ is not accessible experimentally, since both fluorescence and ESR techniques monitor second-rank tensor interactions.

In the simulations the probes are allowed to rotate about their centers and it is therefore expected that they may undergo 'head-over-heels' motion, whereby their long axes tumble with respect to the normal to the bilayer interface and undertake angles over the entire range $0 \leq \beta \leq \pi$. This motion is readily reflected in the decay of the first-rank correlation functions $G^1_{00}(t)$ shown in Figure 5 over the range of burial potential strengths $0 \leq \kappa \leq 0.04kT$. The fast decay of the correlation functions $G^1_{00}(t)$ for probe molecules localized at the center of the bilayer ($\kappa = 0$) indicates that large-scale tumbling motions of the probe axes indeed take place. In marked contrast, the tumbling motions of probe molecules localized in the interfacial regions, e.g., burial potential of strength $\kappa = 0.04kT$, are significantly more constrained. Their correlation function $G^1_{00}(t)$ decays an order

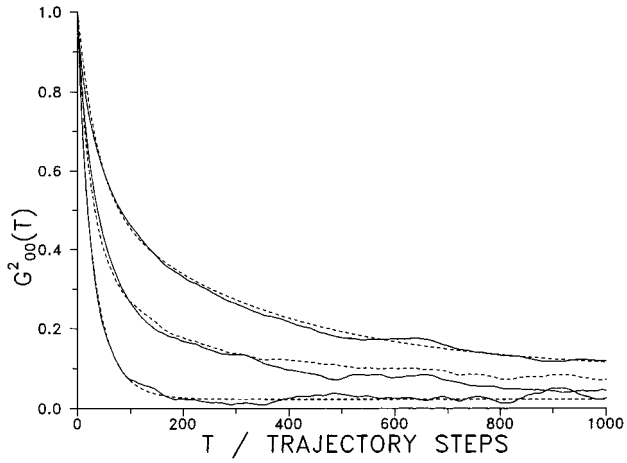

Figure 6. Decay of the second-rank time correlation function $G^2_{00}(t)$ of DPH molecules in the lipid bilayer (continuous lines): population in the middle of the bilayer ($\kappa = 0$) (bottom); population in the interfacial regions ($\kappa = 0.04kT$) (top); a mixed population ($\kappa = 0.03kT$) (center). The fits to the CM model (dashed lines) are shown for the populations in the middle (top) and interfacial regions (bottom) as is the weighted sum of the correlation functions (center).

TABLE 1: Compound Motion Model Parameters Extracted from the Analysis of the Second-Rank Correlation Functions $G^2_{00}(t)$

system	λ_2	λ_4	$D_\perp$ (MCD steps)$^{-1}$	cone angle deg	D_{cone} (MCD steps)$^{-1}$
DPH, $\kappa = 0$	−4.66	0.84	0.0055	60.8	0.018
DPH, $\kappa = 0.04$	1.87	0.09	0.00046	35.5	0.025
perylene z-axis, $\kappa = 0$	1.64	0.09	0.0018	42.1	0.011
perylene z-axis, $\kappa = 0.08$	−1.64	−0.08	0.00034	22.1	0.045

of magnitude more slowly than that for the probes in the bilayer center (Figure 5). Interestingly, the correlation function $G^1_{00}(t)$ for $\kappa = 0.03kT$, when the DPH molecules are almost equally divided between the center of the bilayer and the interfacial regions, is simply half the sum of the functions found for $\kappa = 0$ and $\kappa = 0.04kT$ (Figure 5).

Typical decays of the second-rank correlation functions $G^2_{00}(t)$ evaluated along the MCD trajectories are shown in Figure 6 for probe molecules subjected to a burial potential of strength in the range $0 \leq \kappa \leq 0.04kT$. We note that the correlation function $G^2_{00}(t)$ for $\kappa = 0.03kT$, when the DPH molecules are almost equally divided between the center of the bilayer and the interfacial regions, is simply half the sum of the functions found for $\kappa = 0$ and $\kappa = 0.04kT$ (Figure 6).

We shall here analyze the correlation functions $G^2_{00}(t)$ by fitting them to the predictions of the CM[8,9] in the conventional way. The solution provided by the model is validated by comparing the extracted order parameters $\langle P_2 \rangle$ and $\langle P_4 \rangle$ with the ones obtained directly from averaging the probe molecule orientations along the MCD trajectories. We note that the odd order parameters such as $\langle P_1 \rangle$ and $\langle P_3 \rangle$ are virtually zero, as expected for the symmetric molecules considered here. The best fits to the cases where the probe molecules are primarily localized either in the bilayer center or in the interfacial regions (potential strengths of $\kappa = 0$ and $\kappa = 0.04kT$, respectively) are shown in Figure 6. The corresponding values of the model parameters are given in Table 1. It can be seen that the CM model provides an excellent fit of the data and moreover recovers the values of the order parameters $\langle P_2 \rangle$ and $\langle P_4 \rangle$ obtained by averaging along the MCD trajectories.

As a check of the correctness of the CM description of probe dynamics, the first-rank correlation functions $G^1_{00}(t)$ were

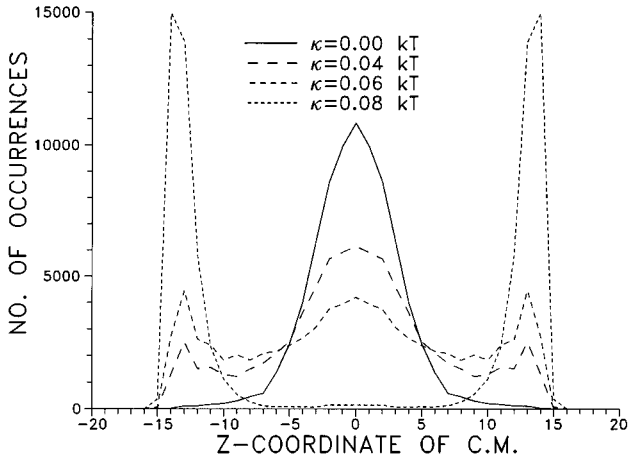

Figure 7. Distribution of the positions of the centers of mass of the model perylene molecules in the bilayer for different strengths of the burial potential.

calculated with the model parameters extracted from the analysis of $G^2_{00}(t)$ and shown in Table 1. It can be seen from Figure 5 that a reasonable agreement is found between the fits and the correlation functions calculated along the MCD trajectories.

We shall now address the question of fitting the second-rank correlation function, $G^2_{00}(t)$ when the bilayer contains equal populations of probes at the center and the two interfacial regions ($\kappa = 0.03kT$) using a single dynamic population model such as the CM. It turns out that the CM model provides good fits, and the values of the order parameters $\langle P_2 \rangle$ and $\langle P_4 \rangle$ recovered from the analysis are in good agreement with the weighted averages of the corresponding order parameters for the two populations. In contrast, the first-rank correlation function, $G^1_{00}(t)$, calculated with the extracted parameters is found to decay much more slowly than that obtained from the simulations.

The ambiguity of the analysis of the second-rank correlation function $G^2_{00}(t)$ is not removed by applying the simple two-population model proposed recently for the analysis of fluorescence depolarization measurements on DPH molecules.[10] This model also provides a good fit for the decay of $G^2_{00}(t)$, but the model parameters extracted from the analysis deviate systematically from those calculated along the MCD trajectory. The model overestimates the fraction of molecules in the interfacial region (70% compared to 48% from the simulations) and underestimates $\langle P_2 \rangle$, 0.24 compared to 0.34 from the MCD trajectories, for the probes in the interfacial region.

These findings indicate an inherent ambiguity in the analysis of fluorescence anisotropy experiments when the probes are distributed in different environments in the bilayer structure. The ambiguity may be removed by using additional independent information, for instance, by explicitly incorporating the dependence of the fluorescence lifetime of DPH on its location in the bilayer.[19] The linking of the fluorescence intensity decay to the fluorescence anisotropy has indeed been exploited in the two-population model.[10]

Perylene Probes. *A. Orientational Distribution Functions*. The simulations were carried out as for DPH above except that only a single model perylene molecule was embedded in the bilayer. The burial potential was taken to act on the center of mass of the molecule as was the case for DPH above. The model perylene molecule has a propensity to remain in the middle of the bilayer and only migrates toward the interface under the action of a relatively strong repulsion potential, $\kappa > 0.06kT$ (Figure 7). This is not surprising in view of its large size. The simulations show that for burial potentials of

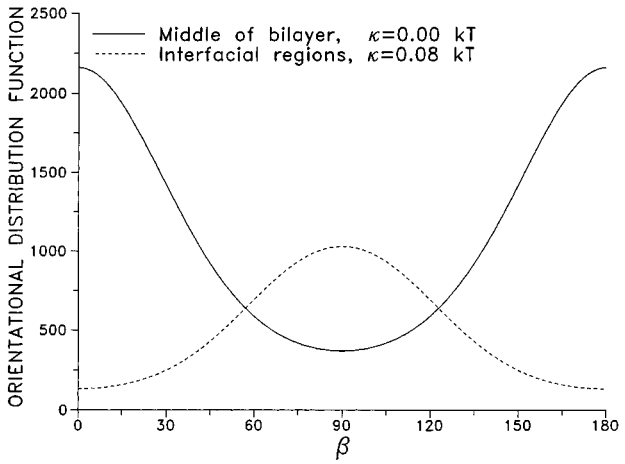

Figure 8. Orientational distribution functions of the model perylene molecules localized in the middle of the bilayer ($\kappa = 0$) and in the interfacial regions ($\kappa = 0.08kT$).

intermediate strength, the center of mass of the molecule is found in two distinct regions of the bilayer and the molecule moves between them on a time scale slow compared to its rotational motions.

We shall now characterize the orientation of the model perylene molecule in the bilayer in terms of the order parameter $\langle P_2 \rangle$ of its *z*-axis, the normal to the molecular plane. The ordering of this axis in the bilayer is only affected by the motion of the molecular plane relative to the interface. It is important to realize that the molecule undergoes rotational diffusion about the *z*-axis, and this motion will average the order parameter of the *x*- or *y*-axis. The orientational behavior of these two axes is monitored experimentally, since the transition dipole moments of perylene lie in the plane of the molecule.[20,21]

The large and positive values of $\langle P_2 \rangle \approx 0.25$ observed for the *z*-axis of the molecule in the middle of the bilayer indicate that it lies with the molecular plane aligned parallel to the bilayer interface. The orientational distribution function is shown in Figure 8. The order parameter decreases sharply to -0.22 on increasing the strength of the burial potential to $\kappa = 0.08kT$. Now the molecule spends over 90% of its time intercalated between the lipid chains and is consequently aligned with its plane perpendicular to the bilayer interface (Figure 8).

B. Reorientational Motions. In dealing with the rotational dynamics of the model perylene molecule, one has to bear in mind that the tumbling motion of the *z*-axis lying normal to the molecular plane is independent of the rotational motion about it. The rotational motion about the *z*-axis is also expected to be fast, since it does not require a change in the size or shape of the free volume region surrounding it. The molecule thus experiences substantially less hindrance for axial rotation than for a reorientation of the its *z*-axis, which implies a sweeping motion of the entire molecule. Since the transition dipole moments of perylene lie in the molecular plane, they will monitor a combination of the two modes of motion. This combined motion is revealed by the time correlation functions for the *x*- or *y*-axis of the model molecule considered here. The simulations show that the correlation functions, $G^1_{00}(t)$ and $G^2_{00}(t)$, for the *x*-axis to be identical with those for the *y*-axis are in line with expectations.

B.1. z-Molecular Axis. The decay of the first-rank correlation function $G^1_{00}(t)$ for the *z*-axis of the molecule, Figure 9, shows that the molecule undergoes reorientational motions similar to those of the long axes of the DPH molecules. This implies that the plane of the perylene molecule tumbles relative to the normal to the bilayer interface. This motion is also

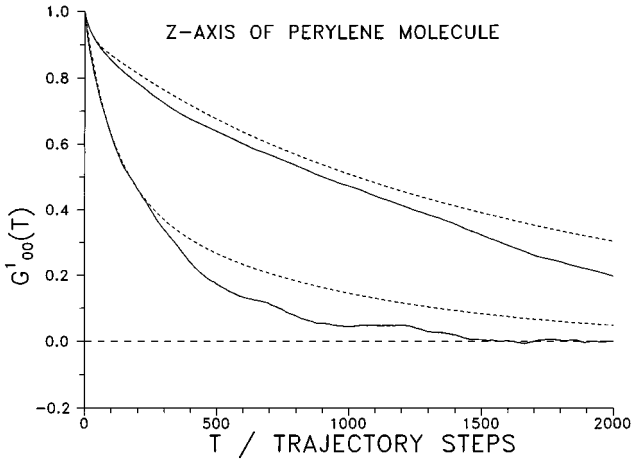

Figure 9. Decay of the first-rank time correlation function $G^1_{00}(t)$ of the *z*-axis of the perylene molecule in the lipid bilayer (continuous lines): population in the middle of the bilayer ($\kappa = 0$) (bottom); population in the interfacial regions ($\kappa = 0.08kT$) (top). The fits to the CM model (dashed lines) are shown for the populations in the middle (top) and interfacial regions (bottom).

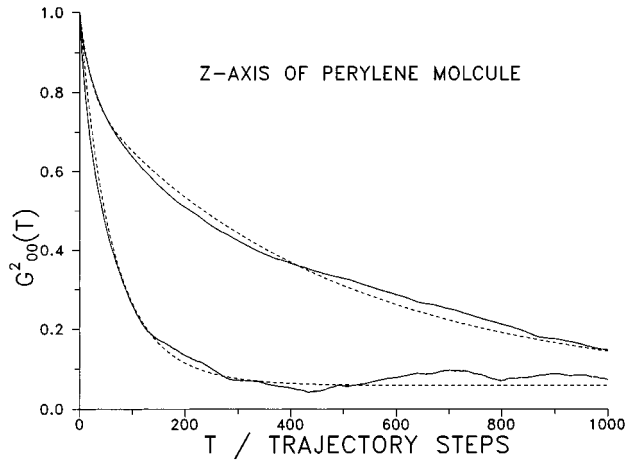

Figure 10. Decay of the second-rank time correlation function $G^2_{00}(t)$ of the *z*-axis of the perylene molecule in the lipid bilayer (continuous lines): population in the middle of the bilayer ($\kappa = 0$) (bottom); population in the interfacial regions ($\kappa = 0.08kT$) (top). The fits to the CM model (dashed lines) are shown for the populations in the middle (top) and interfacial regions (bottom).

reflected in the decay of $G^2_{00}(t)$ (Figure 10). The latter time correlation function is described well by the CM[8,9] model for the two situations where the molecule is localized in the middle of the bilayer (no burial potential) and in the interfacial layers ($\kappa = 0.08kT$) (Figure 10). The recovered model parameters are given in Table 1. As is the case for DPH, the CM model yields a good fit of $G^1_{00}(t)$ with these values. The correlation functions $G^1_{00}(t)$ and $G^2_{00}(t)$ obtained for intermediate strengths of the burial potential are again found to be well described as a simple weighted average of those found for the two populations in the middle of the bilayer and in the interfacial regions.

B.2. x- and y-Molecular Axes. The correlation functions $G^2_{00}(t)$ for the *x*- and *y*-axes of the perylene molecule, Figure 11, decay significantly faster than the corresponding ones for the *z*-axis, since now the fast axial motion contributes to the loss of correlation. We have analyzed these correlation functions for the two situations of localization in the middle of the bilayer ($\kappa = 0$) and in the interfacial regions ($\kappa = 0.08kT$) using the BRD for the sake of simplicity. We have found previously that the effect of the rotation about the *z*-molecular axis is difficult to distinguish from that produced by the fast restricted

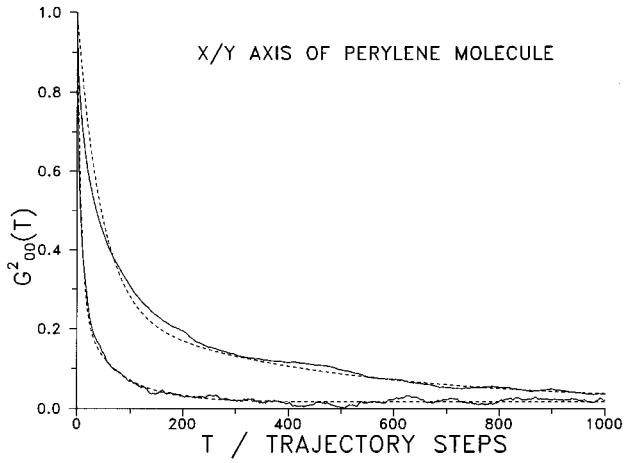

Figure 11. Decay of the second-rank time correlation function $G^2_{00}(t)$ the $x(y)$-axis of the perylene molecule in the lipid bilayer (continuous lines): Population in the middle of the bilayer ($\kappa = 0$) (bottom); population in the interfacial regions ($\kappa = 0.08kT$) (top). The fits to the BRD model (dashed lines) are shown for the populations in the middle (top) and interfacial regions (bottom).

motion within the cavity postulated in the CM model.[13] The BRD[5−7] model will indeed be used for the analysis of the fluorescence anisotropy of perylene in lipid bilayers presented in the accompanying paper.[16] The model fits to $G^2_{00}(t)$ for the two cases of perylene localized in the middle of the bilayer and in the interfacial region are shown in Figure 11.

We shall now consider the case of intermediate burial potential strengths when the perylene molecule is found on average partitioned between the middle of the bilayer and the interfacial regions. The correlation function $G^2_{00}(t)$ can be simply reconstructed as the weighted sum of the corresponding correlation functions for the two regions, as for DPH above. Equally good fits are obtained using the BRD with the orienting potential of eq 2. Remarkably, the recovered values for $\langle P_2 \rangle$ and $\langle P_4 \rangle$ are in good agreement with the weighted averages of the corresponding order parameters for the two populations.

Interestingly, good fits are also obtained using the simple two-population model. However, as was the case for DPH above, the recovered model parameters are different from those obtained from averaging along the MCD trajectory. In particular, we find that the analysis yields two populations, one with order parameters corresponding to those for the perylene molecule in the interfacial region and one exhibiting no orientational order. In addition, the analysis overestimates the fraction of molecules in the ordered population. This appears to be an inherent problem with the model as can be verified by analyzing synthetic data sets. The sets were constructed by the summation of correlation functions calculated using the BRD for probe molecules in the middle of the bilayer and in the interfacial regions. It thus appears that the analysis of experimental fluorescence anisotropy of perylene molecules in lipid bilayers is not straightforward. This is the subject of the accompanying paper.[16]

References and Notes

(1) Silver, B. L. *The Physical Chemistry of Lipids*; Solomon; New York, 1985.

(2) Houslay, M. D.; Stanley, K. K. *Dynamics of Biological Membranes*; Wiley and Son; Chichester, 1982.

(3) *Handbook of Nonmedical Applications of Liposomes: Models for Biological Phenomena;* Barenholz, Y., Lasic, D. D., Eds.; CRC Press; Boca Raton, FL, 1996.

(4) Meirovitch, E.; Freed, J. H. *J. Phys. Chem.* **1980**, *84*, 3295.

(5) Zannoni, C.; Arcioni, A.; Cavatorta, P. *Chem. Phys. Lipids* **1983**, *32*, 179.

(6) Van der Heide, U. A.; Eviatar, H.; Levine, Y. K. *Handbook of Nonmedical Applications of Liposomes: Models for Biological Phenomena*; Barenholz, Y., Lasic, D. D., Eds.; CRC Press: Boca Raton, FL, 1996; Vol. II, pp 61−76.

(7) Nordio, P. L.; Segre, U. *The Molecular Physics of Liquid Crytals*; Luckhurst, G. L., Gray, G. W., Eds.; Academic Press: New York, 1979; pp 411−426.

(8) Van der Sijs, D. A.; Van Faassen, E. E.; Levine, Y. K. *Chem. Phys. Lett.* **1993**, *216*, 559.

(9) Van der Heide, U. A.; Van Zandvoort, M. A. M. J.; Van Faassen, E. E.; Van Ginkel, G.; Levine, Y. K. *J. Fluoresc.* **1994**, *3*, 269.

(10) Van der Heide, U. A.; Van Ginkel, G.; Levine, Y. K. *Chem. Phys. Lett.* **1996**, *253*, 118.

(11) Van der Sijs, D. A.; Levine, Y. K. *J. Chem. Phys.* **1994**, *100*, 6783.

(12) Van der Heide, U. A.; Levine, Y. K. *Biochim. Biophys. Acta* **1994**, *1195*, 1.

(13) Eviatar, H.; Van der Heide, U. A.; Levine, Y. K. *J. Chem. Phys.* **1995**, *102*, 3135.

(14) Nikishaw, K.; Ooi, T. *J. Biochem.* **1986**, *100*, 1043.

(15) Milik, M.; Skolnick, J. *Proteins: Struct. Funct. Genet.* **1993**, *15*, 10.

(16) Van Zandvoort, M. A. M. J.; Gerritsen, H. C.; van Ginkel, G.; Levine, Y. K.; Tarroni, R.; Zannoni, C. *J. Phys. Chem.* **1997**, *101*, 4149.

(17) Allen, M. P.; Tildesley D. J. *Computer simulation of liquids*; Clarendon Press: Oxford, 1987.

(18) Davis, J. H.; Jeffrey, K. R.; Bloom, M. *J. Magn. Reson.* **1978**, *29*, 191.

(19) Gratton, E.; Parasassi, T. *J. Fluoresc.* **1995**, *5*, 51.

(20) Kalman, B.; Clarke, N; Johanssen, B.-Å. *J. Phys. Chem.* **1989**, *93*, 4608.

(21) Christensen, R. L.; Drake, R. C.; Phillips, D. *J. Phys. Chem.* **1986**, *90*, 5960.

(22) Abbreviations used: DPH, 1,6-diphenyl-1,3,5-hexatriene; TMA-DPH, 1-(4-trimethylammonio)-DPH; CSL, 3-doxylcholestan-17β-ol.